Chaos from Hopf bifurcation in a fluid flow experiment

J. Langenberg and G. Pfister
Institute of Experimental and Applied Physics, University of Kiel, 24098 Kiel, Germany

J. Abshagen
Leibniz-Institute for Marine Science, University of Kiel, 24105 Kiel, Germany

(Received 13 April 2004; revised manuscript received 7 July 2004; published 22 October 2004)

Results of an experimental study of a Hopf bifurcation with broken translation symmetry that organizes chaotic homoclinic dynamics from a T^2 torus in a fluid flow as a direct consequence of physical boundaries are presented. It is shown that the central features of the theory of Hopf bifurcation in O(2)-symmetric systems where the translation symmetry is broken are robust and are appropriate to describe the appearance of modulated waves, homoclinic bifurcation, Takens-Bogdanov point, and chaotic dynamics in a fluid flow experiment.

DOI: 10.1103/PhysRevE.70.046209 PACS number(s): 47.20.Ky, 02.30.Oz, 05.45.−a

Ideas from low-dimensional dynamical systems have been very fruitful in order to understand the appearance of complex behavior in spatial extended nonlinear systems [1–3]. Chaotic dynamics often appears in such systems if a control parameter is increased from its critical value of the first bifurcation from the basic state. Homoclinic bifurcations are found to play a crucial role in the organization of low-dimensional chaotic dynamics [4]. They arise from the merging of a period orbit with a saddle-point if a control parameter is varied and originate in the underlying local bifurcation structure of a nonlinear dynamical system [5]. Examples of homoclinic orbits can be found in many nonlinear physical systems, like, e.g., lasers [6], chemical oscillators [7], electronic circuits [8], and fluid flows [9–13]. In order to understand the organization of the bifurcation structure of a spatial extended nonlinear system an in-depth knowledge of the properties of the first bifurcation from the basic state is crucial [1]. Symmetries and symmetry-breaking are important to determine the solution set close to such a bifurcation. Mathematical models of a bifurcation in a spatial extended system often assume translation symmetry. Accompanied with the assumption of a reflection symmetry such a dynamical system is thus considered as being invariant under O(2) symmetry. In the case of Hopf bifurcation with O(2) symmetry either left or right traveling waves or standing waves appear from the basic state [14].

A mathematical model of a bifurcation with O(2) symmetry which results from the assumption of translational symmetry does not reflect necessarily all properties of its physical representation due to the finite spatial extend of the physical system [15]. Therefore a realistic model of a physical system representing a Hopf bifurcation with O(2) symmetry has to cope with the effect of broken translational symmetry.

Bifurcations with broken symmetries due to imperfections have been successfully modeled by adding symmetry-breaking terms to the normal form of the symmetric bifurcation [16]. Examples arise from both imperfect local and imperfect global bifurcations in fluid flows with reflection symmetry (see, e.g., [3,9]).

According to bifurcation theory the normal form of a Hopf bifurcation with O(2) symmetry is qualitatively altered in the presence of imperfections which break the translation symmetry [17–19]. As a consequence of broken translational symmetry the Hopf bifurcation does not only determine the solution structure from the basic state but also predicts higher-order bifurcations away from the critical point in the nonlinear regime.

Instead of traveling and standing waves in the O(2) symmetric case only two types of standing wave solutions appear of the basic state from a Hopf bifurcation with broken translational symmetry. Secondary symmetry breaking bifurcation to traveling wave-type solutions and Hopf bifurcation to modulated waves (MW) occur from these standing waves. The MW form a T^2 torus of standing waves and a very-low-frequency modulation. Furthermore, a Takens-Bogdanov point and homoclinic and heteroclinic bifurcations also occur in the bifurcation structure. They are responsible for the appearance of chaotic dynamics in the normal form [20]. The onset of chaos may thus be considered as a direct consequence of the presence of symmetry-breaking imperfections in a Hopf bifurcation with broken translational symmetry.

In general it is not *a priori* clear that the effect of physical boundaries on the Hopf bifurcation in a fluid flow which is governed by the Navier-Stokes equation correspond to that of a symmetry breaking imperfection term in the normal form of the symmetric bifurcation.

Theoretical work [21,22] and experimental investigations [23,24] on binary mixture convection and experimental studies on nematic liquid crystals under low-frequency ac voltage [25] revealed interesting complex dynamics close to a Hopf bifurcation from which theoretically traveling wave solutions occur. In these systems it is found that nonlinear competition between traveling waves propagating in opposite direction is responsible for the appearance of complex flow states, like, e.g., "blinking states" or irregular "repeated transients."

The aim of this work is to examine whether chaos arises from a Hopf bifurcation with broken translation symmetry in an experimental system due to the presence of physical boundaries.

The system we have chosen is counter-rotating Taylor-Couette flow which is the flow of a viscous liquid in the gap between two concentric rotating cylinders. It is one of the

"classical" hydrodynamic systems for the study of bifurcation with symmetry and chaos. Under the assumption of infinite axial height the basic laminar Couette flow is invariant under the group $O(2)\times SO(2)$ [26,27]. For sufficiently high rates of counter-rotating cylinders spiral vortices occur as the result from a Hopf bifurcation in laminar Couette flow [28–30]. Spiral vortices are traveling waves in axial and rotating waves in azimuthal direction. Experimentally they have been observed first by Snyder [31] and later studied to a larger extend by Andereck *et al.* [32], Tagg *et al.* [33], and Schulz and Pfister [34]. Axially standing wave solutions, called "ribbons," have been observed by Tagg *et al.* [35] in the nonlinear regime and recently by Langenberg *et al.* [36] as the primary pattern from a supercritical Hopf bifurcation in the basic flow.

The experimental setup of the Taylor-Couette system used for this study consists of a viscous fluid confined in the gap between two independently rotating concentric cylinders. The inner cylinder is machined from stainless steel having a radius of $r_i=(12.50\pm0.01)$mm, while the outer cylinder is made from optically polished glass with a radius of $r_o=(25.00\pm0.01)$mm. As a working fluid a silicon oil with the kinematic viscosity $\nu=10.2$ cSt is used. The temperature of the fluid is thermostatically controlled to $(24.00\pm0.01)\,^\circ$C. At top and bottom the fluid is confined by end plates which are held fixed in the laboratory frame. The distance between the plates defines the axial height L of the flow which is adjustable within an accuracy of 0.01 mm. Geometric parameters are the aspect ratio $\Gamma=L/d$, with gap width $d=r_o-r_i$, and the radius ratio $\eta=r_i/r_o$. The radius ratio is held fixed to $\eta=0.5$ for all measurements and the maximum height of the apparatus is $L=250$ mm which correspond to a maximum aspect ratio $\Gamma=20$. As control parameters serve the Reynolds number of the inner (i) and the outer (o) cylinder, $\mathrm{Re}_{i,o}=2\pi d r_{i,o}\Omega_{i,o}/\nu$, where $\Omega_{i,o}$ denote the angular velocity of the inner (i) and the outer (o) cylinder, respectively. We utilize laser Doppler velocimetry (LDV) for measurements of the flow velocity.

Standing waves have been found to supersede spiral vortices as the first time-periodic pattern appearing in counter-rotating Taylor-Couette flow from a Hopf bifurcation for sufficiently small aspect ratio [19,36]. An axial velocity distribution of a standing wave solution measured at $\Gamma=7.3$ for $\mathrm{Re}_i=112.2$ and $\mathrm{Re}_o=-110$ is shown Fig. 1(a). The nodal structure in the distribution provides a clear evidence for a standing wave pattern. A detailed description of this flow state is given in [36]. In the nonlinear regime away from the critical Reynolds number spiral vortices appear. As an example the axial velocity distribution of a spiral vortex flow measured at $\Gamma=7.3, \mathrm{Re}_i=118.2$, and $\mathrm{Re}_o=-110$ is represented in Fig. 1(c). Due to the traveling wave character of spiral vortices the velocity distribution is almost featureless as shown in Fig. 1(c) and described in detail by Schulz and Pfister [34]. Spiral vortices are thus clearly distinguishable from the standing waves.

The axial velocity distribution of a novel flow state is depicted in Fig. 1(b). It has been measured for a Reynolds number within the interval between standing waves shown in Fig. 1(a) and spiral vortices shown in Fig. 1(c). The spatial

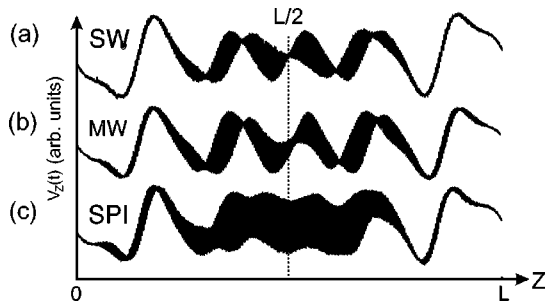

FIG. 1. Axial distributions of axial velocity of (a) standing wave $\mathrm{SW}_0(\Gamma=7.3, \mathrm{Re}_i=112.2, \mathrm{Re}_o=-110)$, (b) modulated wave MW ($\Gamma=7.3, \mathrm{Re}_i=115.3, \mathrm{Re}_o=-110$), and (c) traveling wave SPI ($\Gamma=7.3, \mathrm{Re}_i=118.2, \mathrm{Re}_o=-110$).

characteristic of the flow state is very similar to that of the standing wave flow but with a crucial difference arising in the axial middle of the cylinder. Here, the node that is present in the case of standing waves has disappeared. The velocity distribution is broadened. The broadening arises in the distribution since a spatio-temporal modulation occurs in the flow. The flow state is thus labeled modulated waves (MW).

A time series of the axial velocity of MW recorded 1.2 mm above the axial midplane and at a distance of 1.5 mm from the inner cylinder is shown in Fig. 2(a). In order to visualize the fast dynamics of MW which corresponds to standing waves a single period of the slow oscillation plotted in (a) is depicted in Fig. 2(b). A time-delay reconstruction of the attractor from time series (b) which is shown in Fig. 2(c) and a Poincaré section from an attractor reconstructed from time series (a) which is depicted in (d) demonstrate the quasiperiodic dynamics of MW. Thus the flow evolves dynamically on a T^2-torus. The time delay $\tau=1.1$ s is optimized with

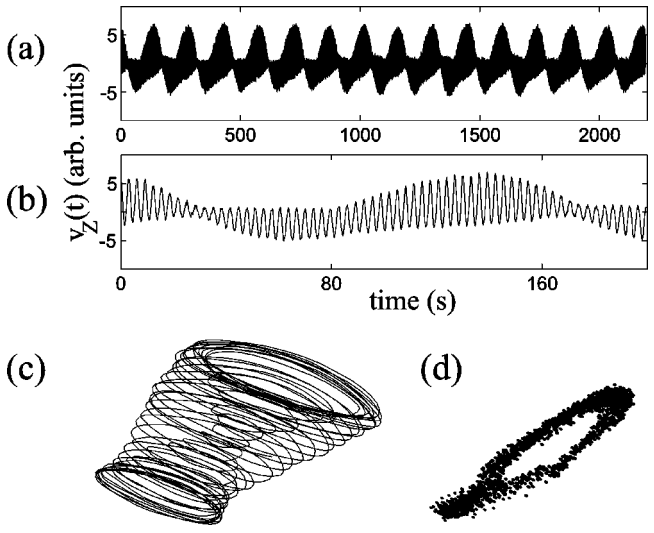

FIG. 2. (a) Axial velocity of a modulated wave measured 1.2 mm above the axial midplane of the system at $\Gamma=7.3, \mathrm{Re}_o=-110$ and $\mathrm{Re}_i=114.5$; (b) a single period of time series plotted in (a); (c) quasiperiodic attractor reconstructed from time series (b) with a time delay $\tau=1.1$ s; (d) Poincaré section of quasiperiodic attractor reconstructed from time series (a) with a time delay $\tau=1.1$ s.

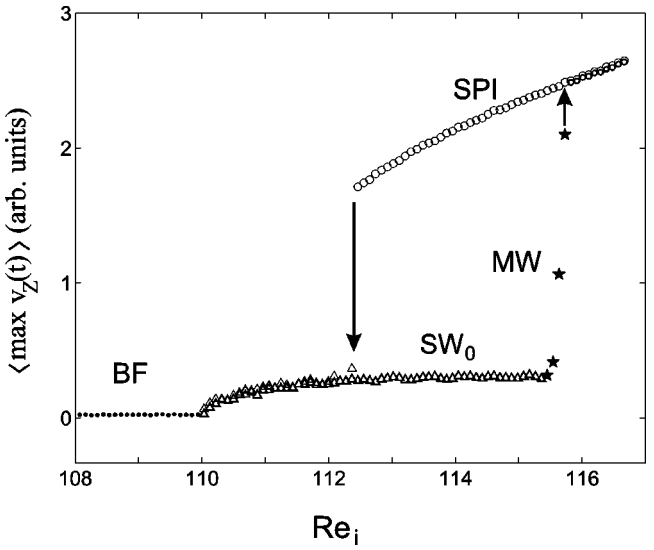

FIG. 3. Bifurcation diagram measured at $\Gamma=7.3$ and $\mathrm{Re}_o=-110$. (·), (△), (★), and (○) represent the mean of the maxima of the axial velocity of BF, SW_0, MW, and SPI, respectively, recorded 1.2 mm above the axial midplane at a distance of 1.5 mm from the inner cylinder.

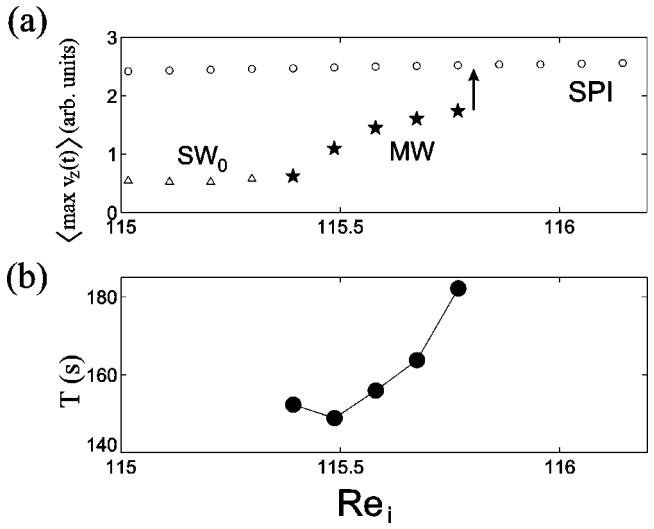

FIG. 4. (a) Bifurcation diagram of modulated waves at $\Gamma=7.3$ and $\mathrm{Re}_o=-110$. (△), (★), and (○) represent the mean of the maxima of the axial velocity of SW_0, MW, and SPI, respectively; (b) modulation period of the standing wave for the same set of parameters.

respect to the experimental time series [37]. The axial midplane does not allow an appropriate measurement of the dynamics on a T^2-torus since the amplitude of standing waves vanishes. The measurement off the midplane introduces an anharmonic behavior of the low-frequency component in the time series as can be seen in Fig. 2. However, the low-frequency component is harmonic if measured directly in the axial midplane. Further flow visualization and LDV measurements in the axial midplane reveal that the modulation results from a time-periodic axial displacement of the wave pattern.

A measurement of the bifurcation diagram of counter-rotating Taylor-Couette flow for $\Gamma=7.3$ and $\mathrm{Re}_o=-110$ is shown in Fig. 3. As a measure of the bifurcation the mean of the maxima of the axial velocity is recorded at a distance of 1.5 mm from the inner cylinder and 1.2 mm above the axial midplane. The transition from the basic flow (BF) to the standing waves (SW_0) occurs via a supercriticial Hopf bifurcation, as shown in detail recently in [36]. Spiral vortices (SPI) exist in this control parameter regime only as a secondary flow. The transition from SPI to SW_0 occurs subcritically at $\mathrm{Re}_c=112.3$ for decreasing Reynolds number as indicated by an arrow in Fig. 3.

For increasing Reynolds number modulated waves (MW) appear supercritically from standing waves (SW_0). Since these waves are only stable within an interval of about one Reynolds number the region of modulated waves have been investigated in a detailed measurement plotted in Fig. 4. Despite the very small stability regime of modulated waves (MW) evidence for a square-root behavior of the modulation amplitude can be found in Fig. 4(a). A power-law behavior is estimated to $\langle \max v_z(t)\rangle \propto \sqrt{\varepsilon}$ with $\varepsilon=(\mathrm{Re}_i-\mathrm{Re}_{i,c})/\mathrm{Re}_{i,c}$. Moreover, the modulation period of the standing wave is finite at onset as depicted in Fig. 4(b). These experimental results provide evidence that modulated waves appear from standing waves as a result of a supercritical Hopf bifurcation at $\mathrm{Re}_c=115.4$. Such a behavior is in agreement with theory of Hopf bifurcation with broken translation symmetry [19].

It can be seen in Fig. 4(a) that the T^2-torus of modulated waves disappears above $\mathrm{Re}_c=115.8$ and the flow undergoes a transition to spiral vortices. This has been indicated by small arrows in Fig. 3 as well as in Fig. 4(a). As shown in Fig. 3 the transition from spiral vortices to standing waves is hysteretic. Details on the nature of the transition from the T^2-torus formed by modulated waves (MW) to spiral vortices (SPI) are represented in Fig. 4(b). It can be seen that the oscillation period of MW increases significantly if the critical Reynolds number is approached. This provides evidence for the appearance of a homoclinic bifurcations from MW. A homoclinic bifurcation from a T^2-torus is an intrinsic part of the theory of Hopf bifurcation with broken translation symmetry. Note, that the experimental accuracy limits the closest distance to the critical point.

Qualitatively similar bifurcation behavior has been found in the flow for different Reynolds number of the outer cylinder and for different aspect ratio. In Fig. 5 the dependence of bifurcation points on the aspect ratio Γ in shown in a stability diagram for $\mathrm{Re}_o=-120$. The critical points are obtained from bifurcation diagrams similar to that shown in Figs. 3 and 4. In Fig. 5 the supercritical Hopf bifurcation from basic flow to SW_0 is indicated by (●) while the supercritical Hopf bifurcation from SW_0 to MW is depicted by (★). The quasiperiodic flow state (MW) occurs only for $\Gamma<7.7$ at $\mathrm{Re}_o=-120$. For $\Gamma>7.7$ SW_0 undergoes a direct transtion to SPI at □ with increasing Re_i. There is strong evidence both from theory [17,19] and from previous experimental studies on standing waves [36] that this transition is due to a subcritical symmetry-breaking bifurcation from SW_0. The hysteretic transition from SPI is indicated by (◇) in Fig. 5. Merging of Hopf bifurcation (★) and subcritical symmetry-breaking bifurcation (□) indicates the existence of a Takens-Bogdanov

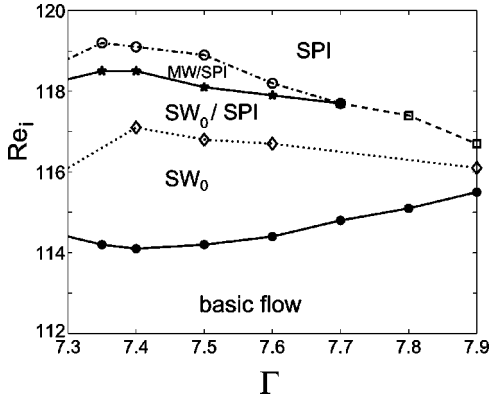

FIG. 5. Stability diagram of flow at $\mathrm{Re}_o=-120$: (●) supercritical Hopf bifurcation to SW_0; (★) supercritcal Hopf bifurcation to MW; (□) subcritcal symmetry-breaking bifurcation from SW_0; (○) homoclinic bifurcation; (◇) subcritcal bifurcation from SPI.

point at $\Gamma=7.7$ in the flow. Such a codimension-2 point gives rise to a heteroclinic bifurcation in a perfectly Z_2-symmetric and a homoclinic bifurcation in an imperfect experimental system [5]. A Takens-Bogdanov point is an intrinsic part of the theory [17,19] and provides thus further evidence that the transition form MW to SPI is due to a homoclinic bifucation at (○).

It has been found theoretically [20] that chaotic homoclinic dynamics also result from Hopf bifurcation with broken translational symmetry. Such a chaotic flow state is found in the experiments in the vicinity of the homoclinic bifurcation. A time series of a chaotic flow at $\mathrm{Re}_o=-130$ is shown in Fig. 6(a). Chaos occurs in the modulation component as indicated in a low-passed filtered version plotted in Fig. 6(b). Further evidence of the chaotic nature of the flow is given in Fig. 6(c) by a reconstruction of an attractor from the filtered time series. An optimal time delay of $\tau=50$ s is used [37]. A Poincaré section of an attractor reconstructed from time series depicted in (a) with a time delay $\tau=1.1$ s is shown in Fig. 6(d). The structure indicates the existence of a low-dimensional chaotic attractor.

We have provided experimental evidence that modulated waves, homoclinic bifurcation, Takens-Bogdanov point and

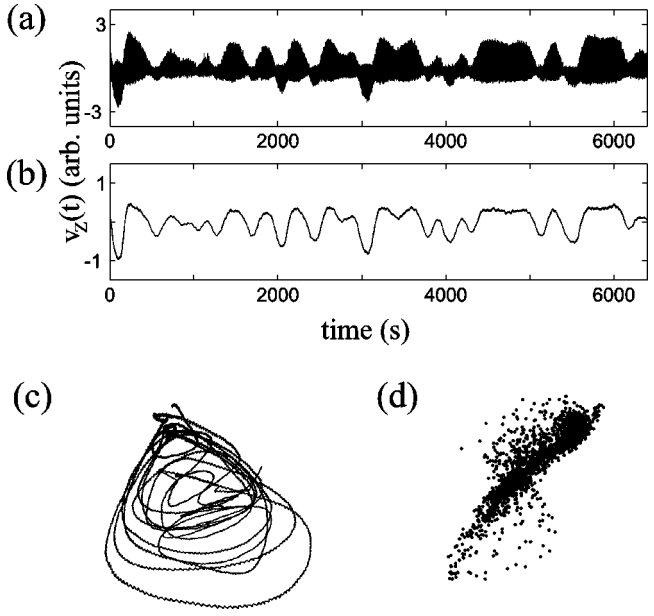

FIG. 6. (a) Axial velocity of a chaotic modulated wave measured 1.2 mm above the axial midplane of the system at $\Gamma=7.3, \mathrm{Re}_o=-130$ and $\mathrm{Re}_i=118.7$; (b) low pass filtered time series; (c) chaotic attractor reconstructed from (b); Poincaré section of chaotic attractor reconstructed from time series (a).

chaotic dynamics arise in a fluid flow from a Hopf bifurcation with broken translation symmetry. Thus the behavior of the fluid flow which is governed by the Navier-Stokes equation can be succesfully modeled by imperfection terms in the normal form of the bifurcation even away from the first critical Reynolds number in the nonlinear regime. We are therefore able to show that the theory of Hopf bifurcation with broken translational symmetry is robust and applicable to Hopf bifurcations in a realistic fluid flow of finite spatial extend.

We thank W. Schumann and H. Horak for technical support. The authors acknowledge support from the "Deutsche Forschungsgemeinschaft" (J.L. and G.P.: research Grant No. PF 210/10-1; JA: SFB460).

[1] M. C. Cross and P. C. Hohenberg, Rev. Mod. Phys. **65**, 851 (1993).
[2] H. L. Swinney and J. P. Gollub, *Hydrodynamic Instabilities and the Transition to Turbulence*, Topics in Applied Physics Vol. 45 (Springer, New York, 1981).
[3] T. Mullin, *The Nature of Chaos* (Clarendon, Oxford, 1993).
[4] P. Glendinning and C. Sparrow, J. Stat. Phys. **35** 645 (1984).
[5] J. Guckenheimer and P. Holmes, *Nonlinear Oscillations, Dynamical Systems, and Bifurcations of Vector Fields*, AMS Vol. 42 (Springer, New York, 1983).
[6] E. Allaria, F. T. Arecchi, A. Di Garbo, and R. Meucci, Phys. Rev. Lett. **86**, 791 (2001).
[7] A. Arnéodo, F. Argoul, J. Elezgaray, and P. Richetti, Physica D **62**, 134 (1993).
[8] P. Glendinning, J. Abshagen, and T. Mullin, Phys. Rev. E **64**, 036208 (2001).
[9] J. Abshagen, G. Pfister, and T. Mullin, Phys. Rev. Lett. **87**, 224501 (2001).
[10] G. Demeter and L. Kramer, Phys. Rev. Lett. **83**, 4744 (1999).
[11] A. M. Rucklidge, Nonlinearity **6**, 1565 (1994).
[12] J. M. Lopez and F. Marques, Phys. Rev. Lett. **85**, 972 (2000).
[13] F. H. Busse, M. Kropp, and M. Zaks, Physica D **61**, 94 (1992).
[14] M. Golubitsky, I. Stewart, and D. G. Schaeffer, *Singularities and Groups in Bifurcation Theory: Vol. 2*, AMS Vol. 69 (Springer, New York, 1988).
[15] T. B. Benjamin, Proc. R. Soc. London, Ser. A **359**, 1 (1978);

359, 27 (1978); K. A. Cliffe, J. J. Kobine, and T. Mullin, *ibid.* **439**, 341 (1992); J. Abshagen, O. Meincke, G. Pfister, K. A. Cliffe, and T Mullin, J. Fluid Mech. **A 476**, 335 (2003).
[16] M. Golubitsky and D. G. Schaeffer, *Singularities and Groups in Bifurcation Theory: Vol. 1*, AMS Vol. 51 (Springer, New York, 1985).
[17] G. Dangelmayr and E. Knobloch, Nonlinearity **4**, 399 (1991).
[18] A. S Landsberg and E. Knobloch, Phys. Rev. E **53**, 3579 (1996).
[19] E. Knobloch and R. Pierce, in *Ordered and Turbulent Patterns in Taylor-Couette Flow*, NATO Advanced Study Institute, edited by C. D. Andereck and F. Hayot, Series B: Physics (Plenum, New York, 1992), Vol. 297.
[20] P. Hirschberg and E. Knobloch, Physica D **90**, 56 (1996).
[21] M. C. Cross, Phys. Rev. Lett. **57**, 2935 (1986); Phys. Rev. A **38**, 3593 (1988).
[22] W. Barten, M. Lücke, M. Kamps, and R. Schmitz, Phys. Rev. E **51**, 5636 (1995).
[23] P. Kolodner, C. M. Surko, and H. Williams, Physica D **37**, 319 (1989).
[24] P. Kolodner, Phys. Rev. E **47**, 1038 (1993).
[25] V. Steinberg, J. Fineberg, E. Moses, and I. Rehberg, Physica D **37**, 359 (1989).
[26] P. Chossat and G. Iooss, *The Couette-Taylor Problem* (Springer, New York, 1994).
[27] M. Golubitsky and I. Stewart, SIAM J. Math. Anal. **17**, 249 (1986); M. Golubitsky and W. F. Langford, Physica D **32**, 362 (1988).
[28] E. R. Krueger, A. Gross, and R. C. Di Prima, J. Fluid Mech. **24**, 521 (1966).
[29] W. F. Langford, R. Tagg, E. J. Koestlich, H. L. Swinney, and M. Golubitsky, Phys. Fluids **31**, 776 (1987).
[30] A. Pinter, M. Lücke, and C. Hoffmann, Phys. Rev. E **67**, 026318 (2003).
[31] H. A. Snyder, Phys. Fluids **11**, 728 (1968).
[32] C. D. Andereck, S. S. Lui, and H. L. Swinney, J. Fluid Mech. **164**, 155 (1986).
[33] R. Tagg, Nonlinear Sci. Today **4**, 1 (1994).
[34] A. Schulz and G. Pfister, in *Physics of Rotating Fluids*, edited by C. Egbers and G. Pfister (Springer, New York, 2002).
[35] R. Tagg, W. S. Edwards, H. L. Swinney, and P. S. Marcus, Phys. Rev. A **39**, 3734 (1989).
[36] J. Langenberg, G. Pfister, and J. Abshagen, Phys. Rev. E **68**, 056308 (2003).
[37] Th. Buzug, T. Reimers, and G. Pfister, Europhys. Lett. **13**, 605 (1990); Th. Buzug and G. Pfister, Phys. Rev. A **45**, 7073 (1992); Physica D **58**, 127 (1992).